Impact of structure and homo-coupling of the central donor unit of small molecule organic semiconductors on solar cell performance†

Pieter Verstappen,[a] Ilaria Cardinaletti,[b] Tim Vangerven,[b] Wouter Vanormelingen,[a] Frederik Verstraeten,[a] Laurence Lutsen,[ac] Dirk Vanderzande,[ac] Jean Manca[d] and Wouter Maes*[ac]

Currently, both low bandgap conjugated polymers and small molecule analogues are employed as electron donor components in state of the art bulk heterojunction organic photovoltaics, providing similar record efficiencies (~10%). However, to evaluate molecular structure-device performance relations and (in particular) the effect of material purity, small molecule chromophores can be considered to be more versatile probes. In the present study, we have synthesized three small molecule donor materials with a varying central electron-rich building block, inspired by the well-known high-performance small molecule p-DTS(FBTTh₂)₂. The influence of this structural modification on the physicochemical material properties, electro-optical characteristics and solar cell performance is analysed. Most importantly, it is shown that the presence of homo-coupled side products generated during Stille cross-coupling reactions – which can be very hard to remove, even for small molecule semiconductors – is detrimental to solar cell performance, with a noticeable effect on the open-circuit voltage.

Introduction

Organic solar cells have attracted a huge amount of attention as a promising "future-proof" energy production technology because of their additional appealing features (compared to standard Si photovoltaics) such as attractive look (different colours and transparency), flexible and light-weight character and the possibility to produce large area devices *via* simple and cheap printing processes.[1] In state of the art bulk hetero-junction organic photovoltaics (BHJ OPV), the photoactive layer consists of two finely intermixed materials, acting as the electron donor and acceptor.[2] Although noteworthy efforts have been conducted to identify viable alternatives for (methano) fullerene n-type materials,[3] phenyl-C₆₁-butyric acid methyl ester (PC₆₁BM) and phenyl-C₇₁-butyric acid methyl ester (PC₇₁BM) are still most often employed. On the other hand, the

donor material has undergone significant evolution over time. During the early days of OPV, almost all studies focused on poly(*p*-phenylene vinylene) (PPV) and poly(3-hexylthiophene) (P3HT) as workhorse conjugated polymers, generating power conversion efficiencies (PCE's) of approximately 3 and 5%, respectively.[4] In recent years, the focus has shifted to push–pull type copolymers. These polymeric semiconductors are composed of electron rich (donor, D) and electron poor (acceptor, A) (heterocyclic) moieties, copolymerized in an alternating fashion by Pd-catalyzed polycondensation reactions. By employing this strategy, intramolecular charge transfer occurs, lowering the bandgap and allowing to harvest significantly more light in comparison to the homopolymers, leading to current reports of solar cell efficiencies approaching and even exceeding 10%.[5]

The advent of the push–pull concept has delivered a toolbox to material chemists not only to effectively lower the bandgap, but also to tune the frontier molecular orbital energy levels rather independently.[1b,6] Nowadays, sufficiently low HOMO–LUMO gaps can already be achieved with relatively short chain "small" molecules. Furthermore, such small molecules offer some specific advantages compared to their polymeric counterparts, *i.e.* less batch-to-batch variation because of their uniform and defined molecular structures and easier purification (although polymer materials may be advantageous in terms of large scale solution processing).[1i,7] Consequently, the interest in small molecule organic solar cells has risen rapidly and PCE's in the proximity of 10% have also been reported recently.[8] Among

a Design & Synthesis of Organic Semiconductors (DSOS), Institute for Materials Research (IMO-IMOMEC), Hasselt University, Universitaire Campus, Agoralaan – Building D, B-3590 Diepenbeek, Belgium. E-mail: wouter.maes@uhasselt.be; Tel: +32 11268312

b Materials Physics Division, Institute for Materials Research (IMO-IMOMEC), Hasselt University, Universitaire Campus, Wetenschapspark 1, B-3590 Diepenbeek, Belgium

c IMEC, IMOMEC, Universitaire Campus, Wetenschapspark 1, B-3590 Diepenbeek, Belgium

d X-LaB, Hasselt University, Universitaire Campus, Agoralaan – Building D, B-3590 Diepenbeek, Belgium

† Electronic supplementary information (ESI) available. See DOI: 10.1039/c6ra06146j

others, Bazan *et al.* developed a D–A–D–A–D strategy based on fluorinated benzothiadiazole (BT) and dithienosilole (DTS), affording the well-known small molecule p-DTS(FBTTh$_2$)$_2$, yielding PCE's exceeding 8%.[8b,9] On the other hand, Chen and co-workers employed a D–A–D concept to achieve OPV devices with similar efficiencies.[8c,10]

Nowadays, it is generally accepted that small changes to the chemical structure of the light-harvesting chromophores can lead to strong variations in final solar cell performance. For example, it was reported that substitution of alkoxy side chains by alkylthio groups effectively improves solar cell efficiency, leading to devices with almost 10% PCE.[8c] It has also been shown that side chain length and position are of major importance for the development of high-performance small molecule organic solar cells.[11] However, the impact of such structural changes is very hard to predict. Additional investigations of structure-device relations are hence certainly still required to make further advances in the field and to evolve from a trial and error to an intelligent design approach. On the other hand, the effect of minor amounts of (organic) impurities on device performance has been underexposed so far and needs further attention, even though it is widely known that purity is of utmost importance in organic electronics. It was for instance shown that the presence of low molar mass materials in polymers can greatly affect both the initial performance and the lifetime of the resulting polymer solar cells.[12] Moreover, although small molecules are often regarded as "easy to purify", Heeger and co-workers already stated that the presence of trace amounts of impurities, which can be hard to remove, significantly influences the solar cell properties, illustrating the need for a better understanding of their effect on the device parameters.[13]

In this work, the central donor unit in the well-known "Bazan" small molecule (p-DTS(FBTTh$_2$)$_2$)[8b,9] was varied and its impact on the physicochemical properties of the resulting materials and the final solar cell characteristics was studied. Three different donor units were chosen, based on their previous use in low bandgap OPV copolymers, *i.e.* 4H-cyclopenta[2,1-*b*:3,4-*b'*]dithiophene (CPDT),[1b,14] N-acyl-substituted dithieno[3,2-*b*:2',3'-*d*]pyrrole (DTP)[15] and thieno[3,2-*b*]thiophene (TT).[16] Incorporation of the CPDT and DTP components allows to study the effect of the bridging atom of these fused bithiophene donor moieties, whereas a more crystalline small molecule is targeted by the introduction of the TT moiety. To guarantee sufficient solubility of the full small molecule series, some additional side chains were introduced on the thiophene units as compared to p-DTS(FBTTh$_2$)$_2$.[8b,9] The novel small molecules were fully characterized and their solar cell properties were determined, along with studies on the film morphology and charge carrier mobility of the donor materials and their blends with PC$_{71}$BM. A noteworthy and strong effect of molecular purity was observed for the DTP-based material, for which homo-coupling of the central donor unit occurred to some extent in the final Stille cross-coupling reaction, with a remarkable detrimental effect on OPV performance.

Results and discussion

Material synthesis and characterization

All three small molecules were prepared following the same synthetic pathway, outlined in Scheme 1. 3,5'-Dihexyl-2,2'-bithiophene (**1**) was synthesized according to a literature procedure and subsequently monostannylated.[17] Stille cross-coupling of precursor **2** with 4,7-dibromo-5-fluorobenzo[*c*][1,2,5]thiadiazole yielded molecule **3**. The targeted small molecules were then obtained *via* Stille cross-coupling of precursor **3** with the bis(trimethylstannyl) derivatives of the appropriate donor molecules. **CPDT(FBTTh$_2$)$_2$** and **DTP(FBTTh$_2$)$_2$** showed excellent solubility in common organic solvents (*e.g.* THF, chloroform and toluene). **TT(FBTTh$_2$)$_2$**, on the other hand, only showed a reasonable solubility in CS$_2$ at room temperature or in chlorinated solvents (*e.g.* 1,1,2,2-tetrachloroethane and chlorobenzene) at elevated temperatures. Since material purity is of major importance for the fabrication of electronic devices, **CPDT(FBTTh$_2$)$_2$** and **DTP(FBTTh$_2$)$_2$** were purified by flash column chromatography (on silica) and recycling preparative size exclusion chromatography (prep-SEC). Due to its limited solubility, **TT(FBTTh$_2$)$_2$** was purified through Soxhlet extraction with methanol, acetone, *n*-hexane and chloroform. ^{1}H NMR analysis indicated high purity of the **CPDT(FBTTh$_2$)$_2$** and **TT(FBTTh$_2$)$_2$** small molecule semiconductors (see ESI†). For **DTP(FBTTh$_2$)$_2$**, some (minor) impurities could be observed (*vide infra*).

The thermal properties of the small molecule series were investigated by rapid heat-cool calorimetry (RHC) (Fig. 1, Table 1). RHC was chosen above regular differential scanning calorimetry (DSC) because of its increased sensitivity to thermal transitions as a result of the fast scanning rates and the low sample amounts required.[18] From the obtained results, it is clear that variation of the central donor unit has a major impact on both the melting temperature (T_m) and melting enthalpy (ΔH_m). As anticipated, the small molecule with the highest degree of crystallinity was acquired by employing thieno[3,2-*b*]thiophene as the central (substituent-free) donor unit.[16] This material showed two melting temperatures, one at a relatively low temperature (120 °C) and a second at higher temperature (230 °C), with the latter exhibiting a large ΔH_m (48.8 J g^{-1}), indicating highly crystalline character. On the other hand, relatively low ΔH_m values were observed for both **CPDT(FBTTh$_2$)$_2$** and **DTP(FBTTh$_2$)$_2$**, demonstrating a more amorphous nature. For **CPDT(FBTTh$_2$)$_2$**, the low melting enthalpy was accompanied by a low melting temperature.

Normalized UV-Vis absorption spectra of the three small molecules in solution (CHCl$_3$) and thin film are shown in Fig. 2. The UV-Vis spectra in chloroform nicely demonstrate that the introduction of more electron rich donor units results in a bathochromic shift. **TT(FBTTh$_2$)$_2$** showed maximum absorption around 550 nm (λ_{max}). When the central donor unit was changed to *N*-acyl-DTP, a red-shift of 30 nm was acquired, and an even higher λ_{max} was obtained when the electron rich CPDT unit was incorporated (Table 1). In thin film, the absorption profiles were broadened and red-shifted. It was also
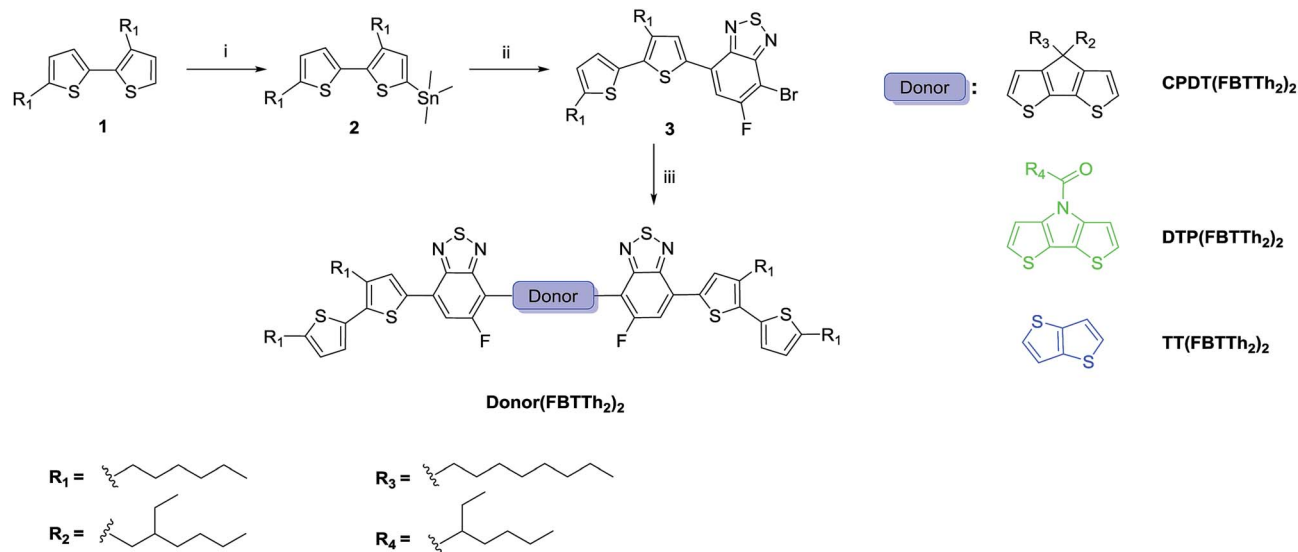
Scheme 1 Synthetic route towards the three small molecules: (i) 1. *n*-BuLi, Et$_2$O, 2. Me$_3$SnCl; (ii) 4,7-dibromo-5-fluorobenzo[*c*][1,2,5]thiadiazole, Pd(PPh$_3$)$_4$, DMF/toluene 1/1, 80 °C, 15 h (64% yield); (iii) bis(trimethylstannyl) derivative of the respective donor molecule, Pd(PPh$_3$)$_4$, DMF/toluene 1/1, 110 °C, 15 h.
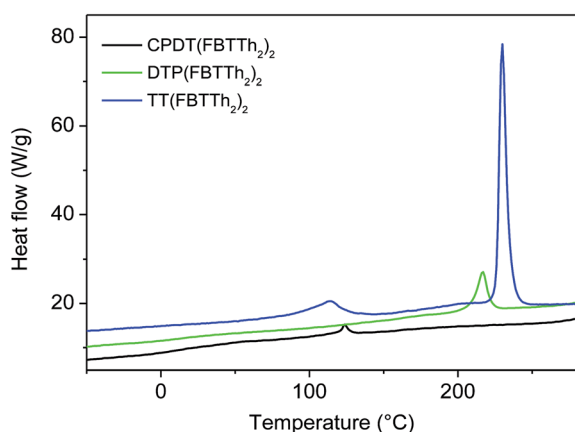

Fig. 1 RHC profiles of the three small molecules (curves shifted vertically for clarity).

observed that the absorption profiles of **CPDT(FBTTh$_2$)$_2$** and **DTP(FBTTh$_2$)$_2$** were more strongly red-shifted in comparison to **TT(FBTTh$_2$)$_2$**, despite the higher degree of crystallinity of the latter, as perceived from RHC. From the UV-Vis spectra in thin film, the optical HOMO–LUMO gaps were determined (Table 1). The smallest optical gap was observed for **DTP(FBTTh$_2$)$_2$** (1.52

eV). Modifying the central donor moiety to CPDT slightly increased the optical gap, which further raised by implementation of TT.

The HOMO and LUMO energy levels of the small molecules were estimated *via* cyclic voltammetry (CV) from the onset of the oxidation and reduction peaks, respectively (Table 1, Fig. S1†). While similar LUMO energy levels were observed for the three small molecules, the HOMO energy levels were (non-surprisingly) significantly influenced by the variation of the central donor unit. Incorporation of TT seemed to yield small molecules with deep HOMO levels, while introduction of the electron rich DTP unit resulted in the highest HOMO level and the smallest electrochemical HOMO–LUMO gap (1.92 eV).

Solar cell analysis

The small molecule electron donor materials were then used to fabricate standard architecture photovoltaic cells, in combination with PC$_{61}$BM or PC$_{71}$BM (Table 2, S1–S3†). The devices were prepared by spin-coating the active layer blends on a PEDOT:PSS (poly(3,4-ethylenedioxythiophene):poly(styrenesulfonate)) hole transport layer, deposited on an ITO (indium tin oxide) transparent electrode. Non-surprisingly, the best processing conditions and optimal donor : acceptor ratio were found to be

Table 1 Thermal, optical and electrochemical properties of the small molecule series

	$T_m{}^a$ (°C)	$\Delta H_m{}^a$ (J g^{-1})	$\lambda_{max}{}^b$ (nm) solution	λ_{max} (nm) film	$E_g^{OP\,c}$ (eV)	HOMO^d (eV)	LUMO^d (eV)	$E_g^{EC\,e}$ (eV)
CPDT(FBTTh$_2$)$_2$	124	2.6	607	677	1.64	−5.43	−3.41	2.02
DTP(FBTTh$_2$)$_2$^{f}	217	11.0	581	681	1.52	−5.35	−3.43	1.92
TT(FBTTh$_2$)$_2$	120/230	11.6/48.8	553	575	1.72	−5.63	−3.38	2.25

^{a} Determined by RHC. ^{b} In chloroform. ^{c} Optical HOMO–LUMO gap, determined by the onset of the solid-state UV-Vis spectrum. ^{d} Determined by CV from the onsets of oxidation and reduction. ^{e} Electrochemical HOMO–LUMO gap. ^{f} Determined for the non-purified sample.
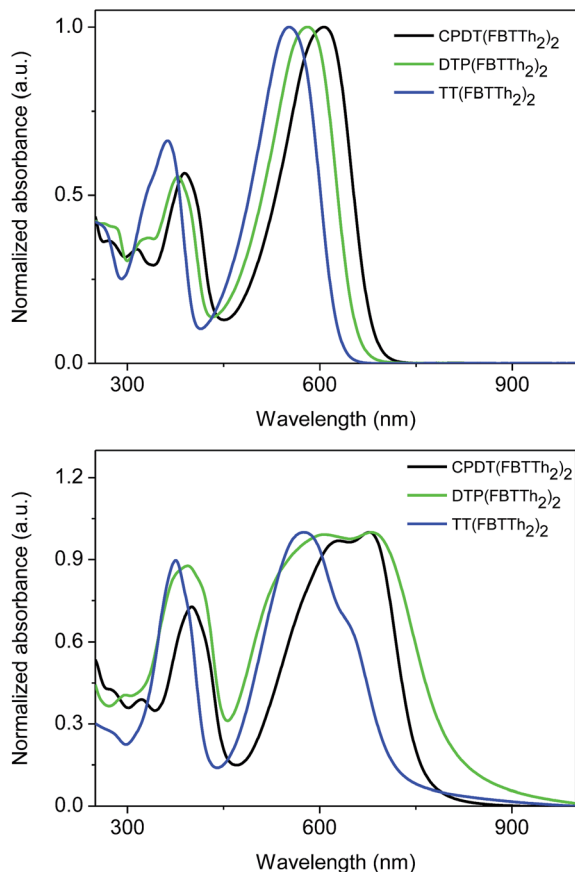
Fig. 2 Normalized UV-Vis absorption spectra for the small molecule series in chloroform solution (top) and in thin film (bottom) (non-purified **DTP(FBTTh₂)₂** was used here).

Fig. 3 *J*–*V* characteristics of the best small molecule solar cells prepared.

different for each donor material, and they are reported in Table 2, together with the average output parameters determining the optimal performance. The current density (*J*)–voltage (*V*) curves of the best performing solar cells are shown in Fig. 3. The use of chlorobenzene (CB) as active layer casting solvent allowed to reach the optimal performance for the solar cells of all three small molecules in blends with $PC_{71}BM$. Due to the low solubility imposed by the TT moiety, **TT(FBTTh₂)₂** had to be deposited from a high temperature CB solution. The use of 1,8-diiodooctane (DIO) allowed for an additional increase of current for the **TT(FBTTh₂)₂**:$PC_{71}BM$ device, reaching a best efficiency of 3.0%. For all compounds, the EQE spectra of the optimal solar
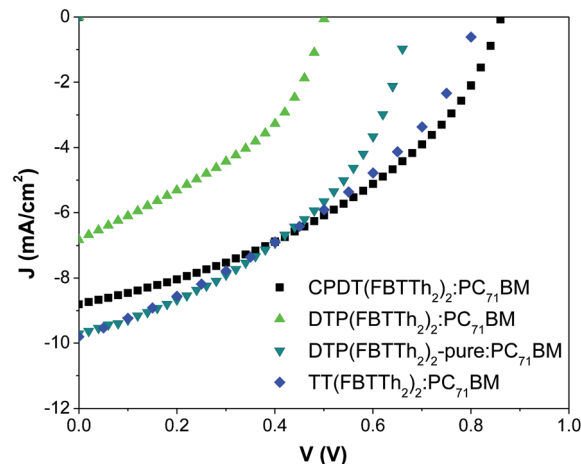
cell devices (Fig. S2†) showed a clear contribution of both the donor material and the fullerene derivative.

Despite extensive optimization of the processing parameters, the performances of all small molecules remained moderate. While for **CPDT(FBTTh₂)₂** and **TT(FBTTh₂)₂** reasonable results were obtained (up to 3% PCE), the solar cell performances of **DTP(FBTTh₂)₂** (PCE around 1%) were very poor. The parameter that contributes most to limiting the final efficiency of the devices presented in this study is the FF, which can possibly be related to the occurrence of recombination processes or to an offset of the hole mobility in the donor material and the electron mobility in the acceptor phase (1×10^{-3} cm² V⁻¹ s⁻¹ for $PC_{71}BM$[19]).[20] To evaluate charge transport, the hole mobility was assessed for the neat small molecule donor materials. Field-effect transistors (FETs) were prepared in the bottom gate bottom contacts configuration by depositing the small molecules from a CB solution on a SiO_2 layer, thermally grown on highly n-doped Si. Gold source and drain contacts were pre-patterned on the substrate, on top of a titanium adhesion layer. Although the observed high threshold voltages (Fig. S3†) suggest the possibility of occurring bias stress,[21] the estimated mobilities do not deviate too far from the values reported for other commonly employed organic semiconductors (~10^{-4} cm² V⁻¹ s⁻¹ for P3HT[22]). Comparable hole mobilities were extracted for **CPDT(FBTTh₂)₂** and **TT(FBTTh₂)₂**, 4.5×10^{-4} and 3.5×10^{-4} cm² V⁻¹ s⁻¹, respectively. Unfortunately, no mobility value

Table 2 Processing and output parameters for the standard architecture organic solar cells based on the three small molecule donor materials

Donor	Acceptor	D : A ratio	Solvent[a]	J_{sc} (mA cm⁻²)	V_{oc} (V)	FF (%)	PCE[b] (%)
CPDT(FBTTh₂)₂	$PC_{71}BM$	1 : 3	CB	8.39	0.85	39.7	2.83 (3.10)
DTP(FBTTh₂)₂[c]	$PC_{71}BM$	1 : 2	CB	6.75	0.50	39.6	1.34 (1.37)
DTP(FBTTh₂)₂-pure	$PC_{71}BM$	1 : 2	CB	8.37	0.67	44.1	2.56 (2.76)
TT(FBTTh₂)₂[d]	$PC_{71}BM$	1 : 2	CB + 0.2% DIO	9.13	0.79	36.4	2.63 (2.96)

[a] CB = chlorobenzene, DIO = 1,8-diiodooctane. [b] Average values over at least 3 devices. The best device performance is shown in parentheses. [c] Before removal of the homo-coupled species. [d] Processed at 85 °C.

could be extracted for **DTP(FBTTh$_2$)$_2$**, due to difficulties in the deposition on the SiO$_2$ substrate.

To examine the photoactive layer blend morphology on the nanoscale, atomic force microscopy (AFM) images were acquired in PeakForce Tapping™ mode. In all cases, the best performing films appeared to be fully intermixed, with little to no evidence of phase separation nor crystallization (Fig. 4).

Homo-coupling defects

Besides the modest FF of all solar cell devices prepared from the novel small molecules, a noteworthy observation is also the low V_{oc} value obtained for the optimal device based on **DTP(FBTTh$_2$)$_2$** (0.50 V, compared to values of 0.79–0.85 V for the other materials), especially since such an inferior value is not expected based on the HOMO energy levels as derived from CV (Table 1). Detailed analysis of the ^{1}H NMR spectrum of **DTP(FBTTh$_2$)$_2$** (see ESI†) revealed the presence of 'small' impurities, which might be causing the V_{oc} drop. Despite the fact that this small molecule was purified by the same two-step procedure as **CPDT(FBTTh$_2$)$_2$** (1× flash column chromatography and 1× prep-SEC), some side product(s) seemed to remain in this sample. To determine the chemical structure of the impurities, MALDI-TOF mass spectrometry analysis was performed (see ESI†). The MALDI spectrum clearly identified the major impurity to be a structure with an additional DTP unit, pointing to the occurrence of homo-coupling of the organotin species during the final Stille cross-coupling reaction (Scheme 1), which leads to a small molecule with two central adjacent DTP units (**DTP(FBTTh$_2$)$_2$-homo**, see Fig. 5).[23] It has to be emphasized that MALDI appears to be an extremely sensitive technique for the detection of molecular (homo-coupling) impurities, whereas ^{1}H NMR analysis only allowed to state that the amount of the side product(s) was below 10%.

It has recently been reported that the presence of homo-coupling in low bandgap copolymers has a detrimental effect on solar cell performance, and especially on V_{oc}.[24] Unfortunately, it can be very hard to identify homo-coupling defects in polymer structures (in a direct way) and its importance hence remains to be elucidated in more detail. To investigate if the low V_{oc} value for the DTP-based small molecule can be correlated to the occurrence of homo-coupling, additional tedious

purification was performed by prep-SEC. Separation of both products was not straightforward due to pronounced tailing on the preparative SEC column (Fig. S4†). The material had to be injected and collected multiple times before the small molecule could be obtained in pure form (denoted as **DTP(FBTTh$_2$)$_2$-pure**). Obviously, the use of such an elaborate purification procedure is not desirable in a commercial setting, clearly demonstrating the need for optimized synthetic protocols affording defect-free materials.

In previous reports, the presence of a low energy tail in the UV-Vis absorption spectrum has been associated to the presence of homo-coupling in low bandgap copolymers.[24] However, despite the red-shifted absorption spectrum of **DTP(FBTTh$_2$)$_2$-homo**, the UV-Vis absorption profiles of **DTP(FBTTh$_2$)$_2$** and **DTP(FBTTh$_2$)$_2$-pure** are nearly identical (Fig. S5†), suggesting that UV-Vis spectroscopy is not the most appropriate technique to decide about the presence of homo-coupled impurities and clearly demonstrating the need to analyse materials by multiple techniques to discover and identify (minor) impurities, which is of course much easier for small molecules.

Subsequently, the solar cell performance of **DTP(FBTTh$_2$)$_2$-pure** was evaluated and the results were compared to the non-purified sample (Table 2, Fig. 3). As anticipated, complete removal of the homo-coupled side product resulted in an enhancement of the V_{oc} of almost 0.2 V to a value of 0.67 V, still below the values for the other two materials but in much better agreement with the trend in HOMO energy levels. Furthermore, besides the V_{oc}, also the J_{sc} and FF benefited from the removal of **DTP(FBTTh$_2$)$_2$-homo**, leading to a final average solar cell efficiency of 2.56%. The purification of the DTP-based small molecule also enabled to deposit it on SiO$_2$ and to extract the hole mobility from FETs. This mobility turned out to be 2.0 × 10^{-5} cm^2 V^{-1} s^{-1}, hence somewhat below the other two small molecules.

To acquire more insight in the nature of the V_{oc} changes, Fourier transform photocurrent spectroscopy (FTPS) studies were performed. It has been widely shown that mixing of an organic semiconductor with a fullerene gives rise to interfacial charge transfer (CT) states, which determine the V_{oc} of organic solar cells.[25] To probe the absorption of the CT state, FTPS spectra were acquired for the optimized devices based on the
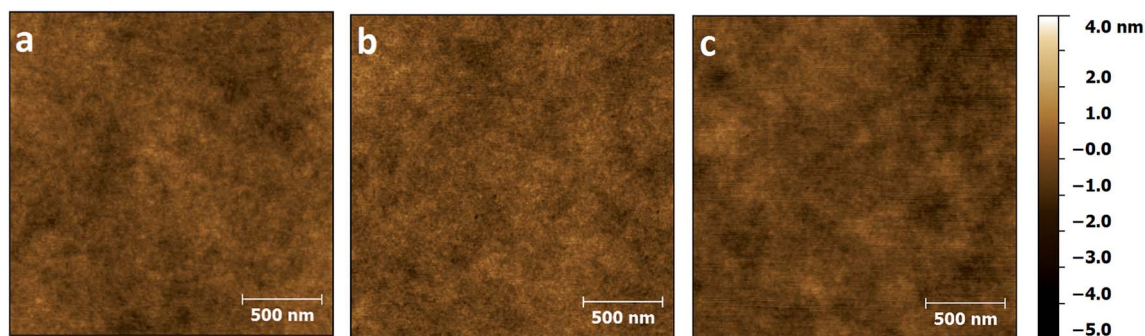

Fig. 4 AFM scans of the active layer blends (resulting in best solar cell performances) based on (a) CPDT(FBTTh$_2$)$_2$, (b) DTP(FBTTh$_2$)$_2$ and (c) TT(FBTTh$_2$)$_2$.
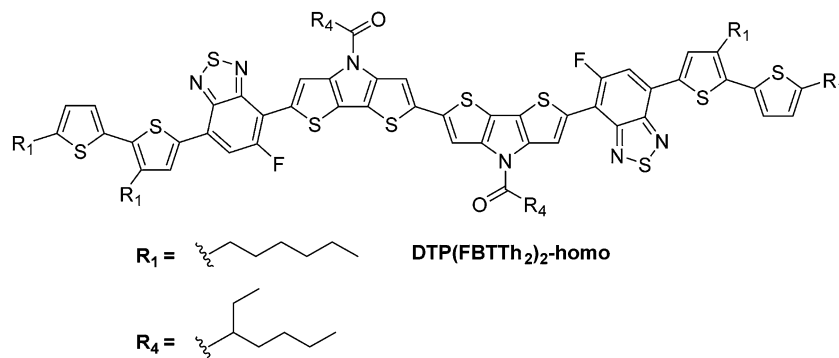
Fig. 5 Structure of the homo-coupled side product **DTP(FBTTh₂)₂-homo**.

three small molecules. The results are shown in Fig. 6, together with the fits of eqn (1) to the CT band.[26]

$$\text{EQE}_{PV}(E) = \frac{f}{E\sqrt{4\pi\lambda kT}} \exp\left(\frac{-(E_{CT} + \lambda - E)^2}{4\lambda kT}\right) \quad (1)$$

Herein, f represents a term that describes the number of CT states, the internal quantum efficiency and the electronic coupling, E_{CT} is the energy of the CT state, λ is related to the width of the CT absorption band, k stands for the Boltzmann constant and T for the temperature.

As expected, the **DTP(FBTTh₂)₂**:PC₇₁BM device exhibits the lowest E_{CT} value (= 1.22 eV, Table S4†) and the **CPDT(FBTTh₂)₂**-PC₇₁BM device the highest (= 1.43 eV), corresponding to the observed trend in V_{oc}. A linear relationship between E_{CT} and V_{oc} has been observed in the past for many different polymer and small molecule OPV systems, where the difference between E_{CT} and qV_{oc} (ΔE) is typically 0.60 ± 0.07 eV, with q being the elementary charge.[27] These energy losses (ΔE) could originate from radiative and non-radiative mechanisms.[26] The best performing (~3% PCE) **CPDT(FBTTh₂)₂** and **TT(FBTTh₂)₂** based devices yield values of 0.58 and 0.54 eV for ΔE, respectively, agreeing with the often observed trend in ΔE. On the other hand,

a remarkably high energy loss of 0.70 eV was observed for the solar cell devices based on non-purified **DTP(FBTTh₂)₂**. After complete removal of **DTP(FBTTh₂)₂-homo**, this energy loss was significantly reduced to 0.55 eV, as the V_{oc} considerably increased and the E_{CT} values for both materials remained similar (Fig. 6 and Table S4†). Burke *et al.* recently developed a model to understand V_{oc} losses.[28] They mention that properties such as the number of CT states, CT lifetime and energetic interfacial disorder can strongly influence V_{oc}. The present results lead to suggest that homo-couplings might have a strong effect on the energetic interfacial disorder, leading to increased V_{oc} losses. Further studies to confirm this hypothesis are still required, however.

Conclusions

Generally, as compared to conjugated polymers, small molecule chromophores have the advantage of a more straightforward and reproducible synthesis, combined with the possibility of purifying these materials more effectively by classical organic synthesis purification methodologies (*e.g.* recrystallization). However, in this study, we have shown that purification of small molecule organic semiconductors is not as straightforward as often projected. Notwithstanding the use of recycling preparative size exclusion chromatography in combination with standard column chromatography, the presence of (minor amounts of) side products could be demonstrated by MALDI-TOF MS analysis. These impurities could be related to the use of the Stille cross-coupling reaction, as they were identified as homo-coupled products. The presence of the homo-coupled species was shown to have a detrimental effect on final solar cell performance. Furthermore, there seems to be a large influence of homo-coupling on the $\Delta E = E_{CT} - V_{oc}$ relationship, as the presence of such side products results in a large deviation from the empirical $\Delta E = 0.6$ eV relation. Therefore, considerable care is required to avoid the formation of homo-coupled side products, something that is currently undervalued in the OPV field.[23,24] In this respect, small molecules are obviously interesting model systems to optimize Stille reactions standardly applied for low bandgap copolymers. On the other hand, the presence of homo-coupled impurities might also have a (strong) effect on OPV device stability,[12] which is currently under investigation within our group.
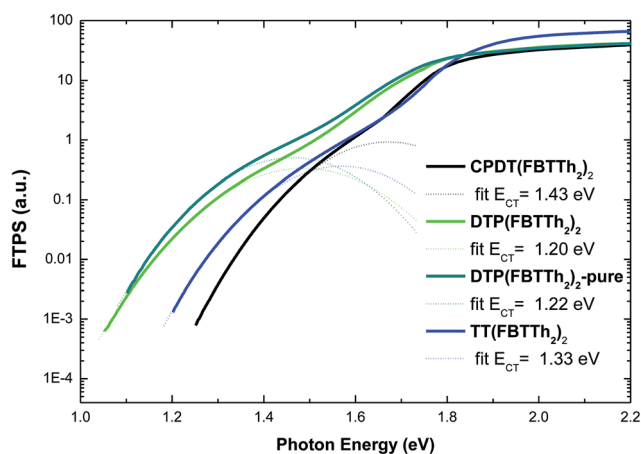

Fig. 6 FTPS spectra of the CT region for optimized devices, with fits to eqn (1) indicated by the dashed lines. The fitting parameters can be found in Table S4.†

Furthermore, it was shown that variation of the central donor unit greatly affects the physicochemical properties of the studied small molecule materials. The crystalline character was modified to a large extent. Despite the large difference in crystallinity, the materials showed comparable solar cell performances (up to ~3% PCE). The considerably lower efficiencies as compared to p-DTS(FBTTh$_2$)$_2$ might be related to the significantly reduced hole mobility for the small molecules reported in this manuscript (with regards to the high mobility, up to 0.14 cm^2 V^{-1} s^{-1}, of p-DTS(FBTTh$_2$)$_2$ (ref. 9)). Finally, it has been confirmed once more that establishing general design rules for small molecule solar cells is not trivial, as optimization of a certain parameter very often leads to (unexpected) negative effects.

Experimental section

Materials and instruments

Preparative (recycling) size exclusion chromatography was performed on a JAI LC-9110 NEXT system equipped with JAIGEL 1*H* and 2*H* columns (eluent CHCl$_3$, flow rate 3.5 mL min^{-1}). NMR spectra were recorded in CDCl$_3$, unless stated otherwise, and chemical shifts (δ, in ppm) were determined relative to the residual CHCl$_3$ (7.26 ppm) absorption or the ^{13}C resonance shift of CDCl$_3$ (77.16 ppm). High resolution electrospray ionization mass spectrometry (ESI-MS) was performed using an LTQ Orbitrap Velos Pro mass spectrometer equipped with an atmospheric pressure ionization source operating in the nebulizer assisted electrospray mode. The instrument was calibrated in the m/z range 220–2000 using a standard solution containing caffeine, MRFA and Ultramark 1621. MALDI-TOF mass spectra were recorded on a Bruker Daltonics Ultraflex II Tof/Tof. 1 μL of the matrix solution (16 mg mL^{-1} DTCB (*trans*-2-[3-(4-*tert*-butylphenyl)-2-methyl-2-propenylidene]malononitrile) in CHCl$_3$) was spotted onto an MTP Anchorchip 600/384 MALDI plate. The spot was allowed to dry and 1 μL of the analyte solution (0.5 mg mL^{-1} in CHCl$_3$) was spotted on top of the matrix. Reported masses are those corresponding to the first peaks of the isotopic patterns. UV-Vis measurements were performed on a VARIAN Cary 500 UV-Vis-NIR spectrophotometer at a scan rate of 600 nm min^{-1}. The films for the UV-Vis measurements were prepared by drop casting a solution of the small molecule in chloroform on a quartz substrate. The solid-state UV-Vis spectra were used to estimate the optical HOMO–LUMO gaps (from the wavelength at the intersection of the tangent line drawn at the low energy side of the absorption spectrum with the x-axis: E_g (eV) = 1240/(wavelength in nm)). Rapid heat-cool calorimetry (RHC) experiments were performed on a prototype RHC of TA Instruments, equipped with liquid nitrogen cooling and specifically designed for operation at high scanning rates.[18] RHC measurements were performed at 250 or 500 K min^{-1} in aluminum crucibles, using helium (6 mL min^{-1}) as a purge gas. Electrochemical measurements (cyclic voltammetry) were performed with an Eco Chemie Autolab PGSTAT 30 potentiostat/galvanostat using a three-electrode microcell with a platinum working electrode, a platinum counter electrode and a Ag/AgNO$_3$ reference electrode (silver wire dipped in a solution of

0.01 M AgNO$_3$ and 0.1 M NBu$_4$PF$_6$ in anhydrous acetonitrile). The reference electrode was calibrated against ferrocene/ferrocenium as an external standard. Samples were prepared by dip coating the platinum working electrode in the respective small molecule solutions (also used for the solid-state UV-Vis measurements). The CV measurements were done on the resulting films with 0.1 M NBu$_4$PF$_6$ in anhydrous acetonitrile as electrolyte solution. To prevent air from entering the system, the experiments were carried out under a curtain of argon. Cyclic voltammograms were recorded at a scan rate of 100 mV s^{-1}. For the conversion of V to eV, the onset potentials of the first oxidation/reduction peaks were used and referenced to ferrocene/ferrocenium, which has an ionization potential of −4.98 eV *vs.* vacuum. This correction factor is based on a value of 0.31 eV for Fc/Fc$^+$ *vs.* SCE[29a] and a value of 4.68 eV for SCE *vs.* vacuum:[29b] $E_{\text{HOMO/LUMO}}(\text{eV}) = -4.98 - E_{\text{onset ox/red}}^{\text{Ag/AgNO}_3}(\text{V}) + E_{\text{onset Fc/Fc}^+}^{\text{Ag/AgNO}_3}(\text{V})$. The reported values (Table 1, Fig. S1†) are the means of the first four redox cycles.

Material synthesis

Unless stated otherwise, all reagents and chemicals were obtained from commercial sources and used without further purification. Solvents were dried by a solvent purification system (MBraun, MB-SPS-800) equipped with alumina columns. Precursors 3,5′-dihexyl-2,2′-bithiophene (**1**),[17] 4,7-dibromo-5-fluorobenzo[*c*][1,2,5]thiadiazole,[30] 2,6-bis(trimethylstannyl)-4-(2′-ethylhexyl)-4-octyl-4*H*-cyclopenta[2,1-*b*:3,4-*b*′]dithiophene,[30] and 2,6-bis(trimethylstannyl)-*N*-(2′-ethylhexanoyl)dithieno[3,2-*b*:2′,3′-*d*]pyrrole[15] were prepared according to literature procedures. 2,5-Bis(trimethylstannyl)thieno[3,2-*b*]thiophene was purchased from Sigma-Aldrich.

[3,5′-Dihexyl-(2,2′-bithiophen)-5-yl]trimethylstannane (2). To an ice cooled solution of 3,5′-dihexyl-2,2′-bithiophene (7.09 g, 21.2 mmol) in dry diethyl ether (30 mL), *n*-BuLi (2.5 M in *n*-hexane; 9.4 mL, 23.5 mmol) was added under a N$_2$ atmosphere. The mixture was stirred for 30 min at 0 °C and Me$_3$SnCl (1 M in THF; 27.4 mL) was added. The solution was allowed to warm gently to room temperature (overnight) and water was added. After extraction with diethyl ether, the organic phase was washed with brine, dried with MgSO$_4$, filtered and evaporated to dryness. The crude product was used without further purification.

4-Bromo-7-[3,5′-dihexyl-(2,2′-bithiophen)-5-yl]-5-fluorobenzo[*c*][1,2,5]thiadiazole (3). [3,5′-Dihexyl-(2,2′-bithiophen)-5-yl]trimethylstannane (1.50 g, 3.02 mmol) and 4,7-dibromo-5-fluorobenzo[*c*][1,2,5]thiadiazole (0.940 g, 3.02 mmol) were dissolved in dry DMF (10 mL) and dry toluene (10 mL) under N$_2$ atmosphere. Pd(PPh$_3$)$_4$ (0.100 g, 0.0865 mmol) was added and the mixture was stirred for 15 h at 80 °C. The solution was allowed to cool to room temperature and water was added. After extraction with diethyl ether, the organic layer was washed with brine, dried with MgSO$_4$, filtered and the solvent was removed under vacuum. Purification by column chromatography (silica, petroleum ether : dichloromethane, 70 : 30) and recycling prep-SEC yielded the pure product as an orange solid (1.10 g, 64%). ^{1}H NMR (400 MHz, CDCl$_3$): δ 7.96 (s, 1H), 7.65 (d, J = 10.1 Hz,

1H), 7.05 (d, J = 3.6 Hz, 1H), 6.77 (d, J = 3.6, 1H), 2.82 (q, J = 7.8 Hz, 4H), 1.71 (quint, J = 7.3 Hz, 4H), 1.48–1.23 (m, 12H), 0.96–0.82 (m, 6H); ^{13}C NMR (100 MHz, CDCl$_3$): δ 160.9 (d, $^1J_{C-F}$ = 251.2 Hz, 1H), 154.4 (d, $^3J_{C-F}$ = 7.4 Hz, 1H), 149.1 (1H), 147.3 (1H), 140.2 (1H), 135.0 (1H), 134.1 (1H), 133.0 (1H), 132.3 (1H), 127.5 (d, $^3J_{C-F}$ = 10.3 Hz, 1H), 126.3 (1H), 124.8 (1H), 115.5 (d, $^2J_{C-F}$ = 30.9 Hz, 1H), 95.8 (d, $^2J_{C-F}$ = 24.8 Hz, 1H), 31.8 (1H), 31.7 (2H), 30.7 (1H), 30.3 (1H), 29.6 (1H), 29.4 (1H), 29.0 (1H), 22.8 (1H), 22.7 (1H), 14.3 (2H).

7,7′-[4-(2′-Ethylhexyl)-4-octyl-4H-cyclopenta[2,1-b:3,4-b′]dithiophene-2,6-diyl]bis{4-[3,5′-dihexyl-(2,2′-bithiophen)-5-yl]-6-fluorobenzo[c][1,2,5]thiadiazole} [CPDT(FBTTh$_2$)$_2$]

General synthesis protocol. Precursor 3 (200 mg, 0.354 mmol), 2,6-bis(trimethylstannyl)-4-(2′-ethylhexyl)-4-octyl-4H-cyclopenta[2,1-b:3,4-b′]dithiophene (126 mg, 0.173 mmol) and Pd(PPh$_3$)$_4$ (10 mg, 0.0087 mmol) were dissolved in a mixture of dry DMF (2 mL) and dry toluene (2 mL). The solution was purged with N$_2$ gas for 30 min and heated to 110 °C for 15 h. The resulting mixture was allowed to cool to room temperature and was precipitated in methanol. After filtration, the crude material was further purified by column chromatography (silica, petroleum ether : dichloromethane, 60 : 40) and recycling prep-SEC and the pure material was collected as a dark blue solid (185 mg, 78%). ^{1}H NMR (400 MHz, CDCl$_3$): δ 8.24 (s, 1H), 8.22 (s, 1H), 7.97 (d, J = 1.3 Hz, 2H), 7.73 (dd, J = 13.4, 1.3 Hz, 2H), 7.06 (d, J = 3.6 Hz, 2H), 6.77 (d, J = 3.6 Hz, 2H), 2.84 (q, J = 7.5 Hz, 8H), 2.16–1.93 (m, 4H), 1.80–1.65 (m, 8H), 1.50–1.27 (m, 25H), 1.24–1.10 (m, 10H), 1.10–0.95 (m, 10H), 0.95–0.83 (m, 12H), 0.83–0.73 (m, 3H), 0.71–0.59 (m, 6H); HRMS (ESI): calcd for C$_{77}$H$_{96}$F$_2$N$_4$S$_8$Na [M + Na]$^+$: 1393.5261, found: 1393.5240; MS (MALDI-TOF) m/z: 1370.5 ([M]$^+$).

1-(2,6-Bis{7-[3,5′-dihexyl-(2,2′-bithiophen)-5-yl]-5-fluorobenzo[c][1,2,5]thiadiazol-4-yl}-4H-dithieno[3,2-b:2′,3′-d]pyrrol-4-yl)-2-ethylhexan-1-one [DTP(FBTTh$_2$)$_2$]. Prepared according to the general synthesis protocol: precursor 3 (200 mg, 0.354 mmol), 2,6-bis(trimethylstannyl)-N-(2′-ethylhexanoyl)dithieno[3,2-b:2′,3′-d]pyrrole (107 mg, 0.170 mmol) and Pd(PPh$_3$)$_4$ (10 mg, 0.0087 mmol) were dissolved in a mixture of dry DMF (2 mL) and dry toluene (2 mL). The **DTP(FBTTh$_2$)$_2$** material was obtained as a dark blue solid (150 mg, 69%). Further purification to remove all residual (homo-coupling) impurities was performed by recycling prep-SEC to afford **DTP(FBTTh$_2$)$_2$-pure** (Fig. S4†). ^{1}H NMR (400 MHz, CS$_2$: CDCl$_3$ 3 : 1) δ 8.90–8.40 (br, 2H), 7.79 (s, 2H), 7.48 (d, J = 13.6 Hz, 2H), 6.91 (d, J = 3.5 Hz, 2H), 6.68 (d, J = 3.5 Hz, 2H), 3.42 (quint, J = 6.5 Hz, 1H), 2.81 (t, J = 7.7 Hz, 4H), 2.67 (t, J = 8.0 Hz, 4H), 2.20–2.05 (m, 2H), 1.97–1.77 (m, 2H), 1.77–1.15 (m, 47H), 1.04 (t, J = 7.2 Hz, 3H), 0.95 (t, J = 6.4 Hz, 12H); HRMS (ESI): calcd for C$_{68}$H$_{77}$F$_2$N$_5$OS$_8$Na [M + Na]$^+$: 1296.3754, found: 1296.3750; MS (MALDI-TOF) m/z: 1273.9 ([M]$^+$).

2,5-Bis{7-[3,5′-dihexyl-(2,2′-bithiophen)-5-yl]-5-fluorobenzo[c][1,2,5]thiadiazol-4-yl}thieno[3,2-b]thiophene [TT(FBTTh$_2$)$_2$]. Precursor 3 (250 mg, 0.442 mmol), 2,5-bis(trimethylstannyl)thieno[3,2-b]thiophene (103 mg, 0.221 mmol) and Pd(PPh$_3$)$_4$ (15 mg, 0.013 mmol) were dissolved in a mixture of dry DMF (2 mL) and dry toluene (2 mL). The solution was purged with N$_2$ gas for 30 min and heated to 110 °C for 15 h. The mixture was cooled down to room temperature and the formed precipitate was

filtered in a Soxhlet thimble. Soxhlet extractions were subsequently performed with methanol, acetone, *n*-hexane and chloroform. The chloroform fraction was precipitated in acetone and the resulting dark purple solid was collected through filtration (181 mg, 74%). Due to its limited solubility in CHCl$_3$, the product could not be further purified by recycling prep-SEC.

^{1}H NMR (400 MHz, CS$_2$: CDCl$_3$ 3 : 1) δ 8.59 (s, 2H), 7.99 (s, 2H), 7.66 (d, J = 13.4 Hz, 2H), 6.97 (d, J = 3.6 Hz, 2H), 6.72 (d, J = 3.6 Hz, 2H), 2.85 (t, J = 7.6 Hz, 4H), 2.79 (t, J = 7.8 Hz, 4H), 1.79–1.67 (m, 8H), 1.52–1.32 (m, 26H), 1.00–0.91 (m, 12H); HRMS (ESI): calcd for C$_{58}$H$_{62}$F$_2$N$_4$S$_8$Na [M + Na]$^+$: 1131.2600, found: 1131.2565; MS (MALDI-TOF) m/z: 1108.3 ([M]$^+$).

Solar cell and FET preparation and characterization

Solar cells in standard architecture were prepared with a layout glass/ITO/PEDOT:PSS/small molecule:methanofullerene/Ca/Al. Substrates with pre-patterned ITO on glass were purchased from Kintec (100 nm, 20 Ohm per sq.) and cleaned through sonication in soap, deionized water, acetone and isopropyl alcohol before proceeding with the spin-coating of PEDOT:PSS (Heraeus Clevios AI 4083). Substrates were subsequently brought inside a N$_2$ filled glovebox and annealed during 10 min at 130 °C to remove residual humidity. All subsequent processing and characterization steps were conducted in inert atmosphere. The active layers in the various blend compositions (see Table 2 and ESI†) were spin-cast on the PEDOT:PSS layer. The optimal concentrations were found to be 35 mg mL^{-1} for **CPDT(FBTTh$_2$)$_2$**, **DTP(FBTTh$_2$)$_2$** and **TT(FBTTh$_2$)$_2$** (in chlorobenzene). In case of additives present in the processing solution, the films were kept under vacuum for a minimum of 2 h to remove residual solvent or additive remainders before thermally evaporating Ca/Al (30/80 nm) stacks as top contacts, defining device areas of 0.03 cm^2 through the use of masks. Electrical characterization was carried out under illumination from a Newport class A solar simulator (model 91195A), calibrated with a silicon solar cell to give a 1 sun AM 1.5G spectrum. EQE measurements were performed with a Newport Apex illuminator (100 W xenon lamp, 6257) as light source, a Newport Cornerstone 130 monochromator and a Stanford SR830 lock-in amplifier for the current measurements. A silicon-calibrated FDS-100 photodiode was employed as a reference cell. J_{EQE} values calculated from the EQE spectra were 8.86, 7.81 and 9.81 mA cm^{-2} for **CPDT(FBTTh$_2$)$_2$**, **DTP(FBTTh$_2$)$_2$-pure** and **TT(FBTTh$_2$)$_2$**, respectively. PeakForce Tapping™ AFM images were acquired with a Bruker Multimode 8 AFM, employing ScanAsyst™. The silicon nitride tip had a spring constant of 4 N m^{-1}. FETs were prepared by spin-coating solutions of **CPDT(FBTTh$_2$)$_2$**, **DTP(FBTTh$_2$)$_2$-pure** and **TT(FBTTh$_2$)$_2$** in chlorobenzene with a concentration of 15, 15 and 8 mg mL^{-1}, respectively, on 200 nm of thermally grown SiO$_2$. The gate contact consisted of highly n-doped Si. Interdigitated source and drain electrodes were pre-patterned, comprising of a stack of Ti/Au (10/100 nm). FET substrates were acquired from Philips. The channel length was 10 μm. Two Keithley 2400 source meters were used to measure the I_{DS} and correct it for leakage

through the gate electrode. All FET preparations and characterizations were carried out in a N_2 filled glovebox. Fourier transform photocurrent spectroscopy (FTPS) was performed using a Thermo Nicolet 8700 FTIR with an external detector. The spectra were recorded with a quartz beamsplitter and appropriate optical bandpass filters to improve the signal to noise ratio. All spectra were corrected for the frequency response. More information can be found in literature.[31]

Acknowledgements

Notes and references

1 Recent reviews on organic solar cells: (a) M. Jørgensen, K. Norrman, S. A. Gevorgyan, T. Tromholt, B. Andreasen and F. C. Krebs, *Adv. Mater.*, 2012, **24**, 580; (b) H. Zhou, L. Yang and W. You, *Macromolecules*, 2012, **45**, 607; (c) Y. Li, *Acc. Chem. Res.*, 2012, **45**, 723; (d) Y. Su, S. Lan and K. Wei, *Mater. Today*, 2012, **15**, 554; (e) R. Søndergaard, M. Hösel, D. Angmo, T. T. Larsen-Olsen and F. C. Krebs, *Mater. Today*, 2012, **15**, 36; (f) R. A. J. Janssen and J. Nelson, *Adv. Mater.*, 2013, **25**, 1847; (g) S. Lizin, S. Van Passel, E. De Schepper, W. Maes, L. Lutsen, J. Manca and D. Vanderzande, *Energy Environ. Sci.*, 2013, **6**, 3136; (h) T. Xu and L. Yu, *Mater. Today*, 2014, **17**, 11; (i) J. Roncali, P. Leriche and P. Blanchard, *Adv. Mater.*, 2014, **26**, 3821; (j) K. A. Mazzio and C. K. Luscombe, *Chem. Soc. Rev.*, 2015, **44**, 78.

2 (a) G. Yu, J. Gao, J. Hummelen, F. Wudl and A. Heeger, *Science*, 1995, **270**, 1789; (b) A. J. Heeger, *Adv. Mater.*, 2014, **26**, 10.

3 (a) C. B. Nielsen, S. Holliday, H.-Y. Chen, S. J. Cryer and I. McCulloch, *Acc. Chem. Res.*, 2015, **48**, 2803; (b) G. Sauvé and R. Fernando, *J. Phys. Chem. Lett.*, 2015, **6**, 3770; (c) S. M. McAfee, J. M. Topple, I. G. Hill and G. C. Welch, *J. Mater. Chem. A*, 2015, **3**, 16393; (d) D. Sun, D. Meng, Y. Cai, B. Fan, Y. Li, W. Jiang, W. Huo, Y. Sun and Z. Wang, *J. Am. Chem. Soc.*, 2015, **137**, 11156; (e) Y.-J. Hwang, B. A. E. Courtright, A. S. Ferreira, S. H. Tolbert and S. A. Jenekhe, *Adv. Mater.*, 2015, **27**, 4578; (f) H. Lin,

S. Chen, Z. Li, J. Yuk Lin Lai, G. Yang, T. McAfee, K. Jiang, Y. Li, Y. Liu, H. Hu, J. Zhao, W. Ma, H. Ade and H. Yan, *Adv. Mater.*, 2015, **27**, 7299.

4 (a) K. M. Coakley and M. D. McGehee, *Chem. Mater.*, 2004, **16**, 4533; (b) S. Günes, H. Neugebauer and N. S. Sariciftci, *Chem. Rev.*, 2007, **107**, 1324; (c) B. C. Thompson and J. M. J. Fréchet, *Angew. Chem., Int. Ed.*, 2008, **47**, 58.

5 (a) L. Ye, S. Zhang, W. Zhao, H. Yao and J. Hou, *Chem. Mater.*, 2014, **26**, 3603; (b) Y. Liu, J. Zhao, Z. Li, C. Mu, W. Ma, H. Hu, K. Jiang, H. Lin, H. Ade and H. Yan, *Nat. Commun.*, 2014, **5**, 5293; (c) Z. He, B. Xiao, F. Liu, H. Wu, Y. Yang, S. Xiao, C. Wang, T. P. Russell and Y. Cao, *Nat. Photonics*, 2015, **9**, 174; (d) J. Subbiah, B. Purushothaman, M. Chen, T. Qin, M. Gao, D. Vak, F. H. Scholes, X. Chen, S. E. Watkins, G. J. Wilson, A. B. Holmes, W. W. H. Wong and D. J. Jones, *Adv. Mater.*, 2015, **27**, 702; (e) W. Yue, R. Shahid Ashraf, C. B. Nielsen, E. Collado-Fregoso, M. R. Niazi, S. Amber Yousaf, M. Kirkus, H.-Y. Chen, A. Amassian, J. R. Durrant and I. McCulloch, *Adv. Mater.*, 2015, **27**, 4702; (f) G. Pirotte, J. Kesters, P. Verstappen, S. Govaerts, J. Manca, L. Lutsen, D. Vanderzande and W. Maes, *ChemSusChem*, 2015, **8**, 3228.

6 (a) R. L. Uy, S. C. Price and W. You, *Macromol. Rapid Commun.*, 2012, **33**, 1162; (b) M. Jeffries-EL, B. M. Kobilka and B. J. Hale, *Macromolecules*, 2014, **47**, 7253.

7 (a) A. Mishra and P. Bäuerle, *Angew. Chem., Int. Ed.*, 2012, **51**, 2020; (b) Y. Chen, X. Wan and G. Long, *Acc. Chem. Res.*, 2013, **46**, 2645.

8 (a) Y. Liu, C.-C. Chen, Z. Hong, J. Gao, Y. M. Yang, H. Zhou, L. Dou, G. Li and Y. Yang, *Sci. Rep.*, 2013, **3**, 3356; (b) A. K. K. Kyaw, D. H. Wang, V. Gupta, J. Zhang, S. Chand, G. C. Bazan and A. J. Heeger, *Adv. Mater.*, 2013, **25**, 2397; (c) B. Kan, Q. Zhang, M. Li, X. Wan, W. Ni, G. Long, Y. Wang, X. Yang, H. Feng and Y. Chen, *J. Am. Chem. Soc.*, 2014, **136**, 15529; (d) B. Kan, M. Li, Q. Zhang, F. Liu, X. Wan, Y. Wang, W. Ni, G. Long, X. Yang, H. Feng, Y. Zuo, M. Zhang, F. Huang, Y. Cao, T. P. Russell and Y. Chen, *J. Am. Chem. Soc.*, 2015, **137**, 3886; (e) K. Sun, Z. Xiao, S. Lu, W. Zajaczkowski, W. Pisula, E. Hanssen, J. M. White, R. M. Williamson, J. Subbiah, J. Ouyang, A. B. Holmes, W. W. H. Wong and D. J. Jones, *Nat. Commun.*, 2015, **6**, 6013; (f) L. Yuan, Y. Zhao, J. Zhang, Y. Zhang, L. Zhu, K. Lu, W. Yan and Z. Wei, *Adv. Mater.*, 2015, **27**, 4229.

9 (a) T. S. van der Poll, J. A. Love, T.-Q. Nguyen and G. C. Bazan, *Adv. Mater.*, 2012, **24**, 3646; (b) A. K. K. Kyaw, D. H. Wang, V. Gupta, W. L. Leong, L. Ke, G. C. Bazan and A. J. Heeger, *ACS Nano*, 2013, **7**, 4569; (c) J. E. Coughlin, Z. B. Henson, G. C. Welch and G. Bazan, *Acc. Chem. Res.*, 2014, **47**, 257.

10 (a) J. Zhou, Y. Zuo, X. Wan, G. Long, Q. Zhang, W. Ni, Y. Liu, Z. Li, G. He, C. Li, B. Kan, M. Li and Y. Chen, *J. Am. Chem. Soc.*, 2013, **135**, 8484; (b) Y. Chen, X. Wan and G. Long, *Acc. Chem. Res.*, 2013, **46**, 2645.

11 (a) J. Min, Y. N. Luponosov, A. Gerl, M. S. Polinskaya, S. M. Peregudova, P. V. Dmitryakov, A. V. Bakirov, M. A. Shcherbina, S. N. Chvalun, S. Grigorian, N. Kaush-Busies, S. A. Ponomarenko, T. Ameri and C. J. Brabec, *Adv. Energy Mater.*, 2014, **5**, 1301234; (b) V. S. Gevaerts, E. M. Herzig, M. Kirkus, K. H. Hendriks, M. M. Wienk,

J. Perlich, P. Müller-Buschbaum and R. A. J. Janssen, *Chem. Mater.*, 2014, **26**, 916; (*c*) M. Jung, Y. Yoon, J. H. Park, W. Cha, A. Kim, J. Kang, S. Gautam, D. Seo, J. H. Cho, H. Kim, J. Y. Choi, K. H. Chae, K. Kwak, H. J. Son, M. J. Ko, H. Kim, D.-K. Lee, J. Y. Kim, D. H. Choi and B. Kim, *ACS Nano*, 2014, **8**, 5988; (*d*) H. Qin, L. Li, F. Guo, S. Su, J. Peng, Y. Cao and X. Peng, *Energy Environ. Sci.*, 2014, **7**, 1397.

12 (*a*) W. R. Mateker, J. D. Douglas, C. Cabanetos, I. T. Sachs-Quintana, J. A. Bartelt, E. T. Hoke, A. El Labban, P. M. Beaujuge, J. M. J. Fréchet and M. D. McGehee, *Energy Environ. Sci.*, 2013, **6**, 2529; (*b*) J. Kong, S. Song, M. Yoo, G. Y. Lee, O. Kwon, J. K. Park, H. Back, G. Kim, S. H. Lee, H. Suh and K. Lee, *Nat. Commun.*, 2014, **5**, 5688.

13 W. L. Leong, G. C. Welch, L. G. Kaake, C. J. Takacs, Y. Sun, G. C. Bazan and A. J. Heeger, *Chem. Sci.*, 2012, **3**, 2103.

14 (*a*) J. Peet, J. Y. Kim, N. E. Coates, W. L. Ma, D. Moses, A. J. Heeger and G. C. Bazan, *Nat. Mater.*, 2007, **6**, 497; (*b*) A. P. Zoombelt, S. G. J. Mathijssen, M. G. R. Turbiez, M. M. Wienk and R. A. J. Janssen, *J. Mater. Chem.*, 2010, **20**, 2240; (*c*) S. Albrecht, S. Janietz, W. Schindler, J. Frisch, J. Kurpiers, J. Kniepert, S. Inal, P. Pingel, K. Fostiropoulos, N. Koch and D. J. Neher, *J. Am. Chem. Soc.*, 2012, **134**, 14932; (*d*) S. Van Mierloo, A. Hadipour, M.-J. Spijkman, N. Van den Brande, B. Ruttens, J. Kesters, J. D'Haen, G. Van Assche, D. M. de Leeuw, T. Aernouts, J. Manca, L. Lutsen, D. Vanderzande and W. Maes, *Chem. Mater.*, 2012, **24**, 587; (*e*) M. Horie, J. Kettle, C.-Y. Yu, L. A. Majewski, S.-W. Chang, J. Kirkpatrick, S. M. Tuladhar, J. Nelson, B. R. Saunders and M. L. Turner, *J. Mater. Chem.*, 2012, **22**, 381.

15 (*a*) W. Vanormelingen, J. Kesters, P. Verstappen, J. Drijkoningen, J. Kudrjasova, S. Koudjina, V. Liégeois, B. Champagne, J. Manca, L. Lutsen, D. Vanderzande and W. Maes, *J. Mater. Chem. A*, 2014, **2**, 7535; (*b*) J. Kesters, P. Verstappen, W. Vanormelingen, J. Drijkoningen, T. Vangerven, L. Marin, B. Champagne, J. Manca, L. Lutsen, D. Vanderzande and W. Maes, *Sol. Energy Mater. Sol. Cells*, 2015, **136**, 70.

16 (*a*) H. Bronstein, Z. Chen, R. S. Ashraf, W. Zhang, J. Du, J. R. Durrant, P. S. Tuladhar, K. Song, S. E. Watkins, Y. Geerts, M. M. Wienk, R. A. J. Janssen, T. Anthopoulos, H. Sirringhaus, M. Heeney and I. McCulloch, *J. Am. Chem. Soc.*, 2011, **133**, 3272; (*b*) J. C. Bijleveld, R. A. M. Verstrijden, M. M. Wienk and R. A. J. Janssen, *J. Mater. Chem.*, 2011, **21**, 9224; (*c*) Y. S. Choi and W. H. Jo, *Org. Electron.*, 2013, **14**, 1621.

17 C.-Y. Kuo, W. Nie, H. Tsai, H.-J. Yen, A. D. Mohite, G. Gupta, A. M. Dattelbaum, D. J. William, K. C. Cha, Y. Yang, L. Wang and H.-L. Wang, *Macromolecules*, 2014, **47**, 1008.

18 (*a*) R. L. Danley, P. A. Caulfield and S. R. Aubuchon, *Am. Lab.*, 2008, **40**, 9; (*b*) T. Ghoos, N. Van den Brande, M. Defour, J. Brassinne, C.-A. Fustin, J.-F. Gohy, S. Hoeppener, U. S. Schubert, W. Vanormelingen, L. Lutsen, D. J. Vanderzande, B. Van Mele and W. Maes, *Eur. Polym. J.*, 2014, **53**, 206.

19 B. Ebenhoch, S. A. J. Thomson, K. Genevičius, G. Juška and I. D. W. Samuel, *Org. Electron.*, 2015, **22**, 62.

20 L. J. A. Koster, V. D. Mihailetchi and P. W. M. Blom, *Appl. Phys. Lett.*, 2006, **88**, 052104.

21 A. Salleo and R. A. Street, *J. Appl. Phys.*, 2003, **94**, 471.

22 J.-C. Bolsée and J. Manca, *Synth. Met.*, 2011, **161**, 789.

23 (*a*) P. Espinet and A. M. Echavarren, *Angew. Chem., Int. Ed.*, 2004, **43**, 4704; (*b*) A. E. Rudenko and B. C. Thompson, *J. Polym. Sci., Part A: Polym. Chem.*, 2015, **53**, 135.

24 (*a*) K. H. Hendriks, W. Li, G. H. L. Heintges, G. W. P. van Pruissen, M. M. Wienk and R. A. J. Janssen, *J. Am. Chem. Soc.*, 2014, **136**, 11128; (*b*) L. Lu, T. Zheng, T. Xu, D. Zhao and L. Yu, *Chem. Mater.*, 2015, **27**, 537; (*c*) T. Vangerven, P. Verstappen, J. Drijkoningen, W. Dierckx, S. Himmelberger, A. Salleo, D. Vanderzande, W. Maes and J. V. Manca, *Chem. Mater.*, 2015, **27**, 3726; (*d*) J. Kudrjasova, J. Kesters, P. Verstappen, J. Brebels, T. Vangerven, I. Cardinaletti, J. Drijkoningen, H. Penxten, J. Manca, L. Lutsen, D. Vanderzande and W. Maes, *J. Mater. Chem. A*, 2016, **4**, 791.

25 K. Vandewal, K. Tvingstedt, A. Gadisa, O. Inganäs and J. V. Manca, *Nat. Mater.*, 2009, **8**, 904.

26 K. Vandewal, K. Tvingstedt, A. Gadisa, O. Inganäs and J. V. Manca, *Phys. Rev. B: Condens. Matter Mater. Phys.*, 2010, **81**, 125204.

27 K. R. Graham, P. Erwin, D. Nordlund, K. Vandewal, R. Li, G. O. N. Ndjawa, E. T. Hoke, A. Salleo, M. E. Thompson, M. D. McGehee and A. Amassian, *Adv. Mater.*, 2013, **25**, 6076.

28 T. M. Burke, S. Sweetnam, K. Vandewal and M. D. McGehee, *Adv. Energy Mater.*, 2015, **5**, 1500123.

29 (*a*) J. Bard and L. R. Faulkner, *Electrochemical methods: fundamentals and applications*, Wiley, 2nd edn, 2001; (*b*) S. Trasatti, *Pure Appl. Chem.*, 1986, **58**, 955.

30 P. Verstappen, J. Kesters, W. Vanormelingen, G. H. L. Heintges, J. Drijkoningen, T. Vangerven, L. Marin, S. Koudjina, B. Champagne, J. Manca, L. Lutsen, D. Vanderzande and W. Maes, *J. Mater. Chem. A*, 2015, **3**, 2960.

31 K. Vandewal, L. Goris, I. Haeldermans, M. Nesládek, K. Haenen, P. Wagner and J. V. Manca, *Thin Solid Films*, 2008, **516**, 7135.